Available at www.sciencedirect.com

ScienceDirect

journal homepage: www.elsevier.com/locate/he

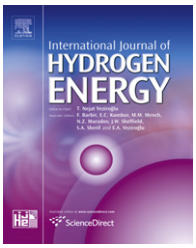

Static and dynamic hydrogen adsorption on Pt/AC and MOF-5

*Andrew C. Chien, Steven S.C. Chuang**

Department of Chemical and Biomolecular Engineering, FirstEnergy Advanced Energy Research Center, The University of Akron, 200 E Buchtel Commons, Akron, OH 44325-3906, USA

ARTICLE INFO

Article history:
Received 9 November 2010
Received in revised form
25 December 2010
Accepted 9 January 2011
Available online 29 March 2011

Keywords:
Dynamic method
Langmuir adsorption isotherm
Breakthrough curves
Temperature variable adsorption
Hydrogen storage
Spillover

ABSTRACT

Hydrogen adsorption has been studied by static and dynamic methods on activated carbon (AC), platinum/activated carbon (Pt/AC), metal organic frameworks (MOF-5), and Pt/AC_MOF-5.The static method showed that all of adsorbents used in this study exhibited a Langmuir (type I) adsorption isotherm at 77 K and a linear function of hydrogen partial pressure at 298 K. The dynamic method produced breakthrough curves, indicating (i) slow rate of hydrogen diffusion in the densely packed activated carbon and Pt/AC beds and (ii) high rate of hydrogen diffusion in the loosely packed bed with large MOF-5 crystallites. Temperature variable adsorption resulted in the higher hydrogen uptake on Pt/AC than other adsorbents. The results suggested that temperature variable adsorption enhanced the hydrogen storage process by (i) initiating hydrogen dissociation at high temperature and (ii) facilitating spillover at low temperature on Pt/AC.

1. Introduction

Hydrogen storage materials have been extensively studied by static adsorption methods. Static methods operate in either volumetric or gravimetric modes under equilibrium conditions [1,2]. The static method serves as an excellent approach to determine the number of adsorption sites, but provides little information on dynamic behaviors of hydrogen uptake/release processes. Practical hydrogen storage materials must possess not only high storage capacity but also rapid uptake/release rates. A potentially effective approach to investigate the process of hydrogen uptake/release is the dynamic approach which involves (i) varying either the inlet H_2 concentration or adsorbent temperatures, and (ii) simultaneously monitoring a real-time response. This approach could provide valuable information of hydrogen storage and dynamic behavior of uptake/release.

We have employed a dynamic adsorption method to study hydrogen adsorption on Pt/AC (activated carbon) and MOFs (metal-organic frameworks). Nanostructure materials such as activated carbon [3–5] and MOFs [6–9] with a high specific surface area (SSA) have been shown to exhibit high hydrogen storage capacity. Studies on various nanoscale carbon materials consisting of activated carbon [10–12] and carbon nanofibers [13–15] have indicated that hydrogen storage capacity is correlated with the pore volume and the SSA.Hydrogen storage capacity as high as 6 wt% have been reported for MOFs with a SSA of 3000 m^2/g at 77 K [16]. Increasing temperature to 298 K reduces the hydrogen storage capacity to less than 1 wt % [17–20]. One approach to increasing hydrogen storage capacities at ambient conditions is to provide the sites for hydrogen adsorption by doping carbon materials with transition metals [21–24] and by mixing MOFs (metal-organic frameworks) with metal sites through building of the carbon bridge [25–27]. Molecule hydrogen could dissociate on the metal sites and then spillover (i.e., migration) from metal sites to the carbon or MOF surface.

* *Corresponding author*. Tel.: +1 330 972 6993; fax: +1 330 972 5856.
E-mail address: schuang@uakron.edu (S.S.C. Chuang).

0360-3199/$ – see front matter Copyright © 2011, Hydrogen Energy Publications, LLC. Published by Elsevier Ltd. All rights reserved.
doi:10.1016/j.ijhydene.2011.01.037

Nomenclature

AC	activated carbon
Ar	argon
BET	Brunauer-Emmet-Teller
C	concentrations
D	deuterium
DMF	N, N'-dimethylforamide
F(t)	$[C(t)-C_0]/[C_\infty - C_0]$, normalized concentration
h	hour
H	hydrogen
He	helium
H-K	Horvath–Kawazoe method
m/e	mass/electron ratio
MOFs or MOF-5	metal organic frameworks
MS	mass spectroscopy
Pt	platinum
Pt/AC	platinum/activated carbon
Pd/AC	pladium/activated carbon
SSA	specific surface area
T	temperature, K
t	time, min
TVA/D	temperature variable adsorption/desorption
θ_H, θ_D	sites coverage

The dynamic adsorption method offers great advantages on adjusting adsorption parameters (i.e. concentration, temperature and pressure) and allows determination of kinetic characteristics of hydrogen adsorption. This paper reported results of a study on MOF-5, Pt/AC_MOF-5, AC, and Pt/AC with three distinct dynamic adsorption methods: (i) a pulse of H_2 into an inert gas stream, (ii) a gas switching between H_2 and an inert gas stream, and (iii) a temperature variable adsorption (i.e. to adsorb during cooling from 298 to 77 K). Dynamic adsorption methods show hydrogen diffusion and adsorption behaviors by breakthrough curves during uptake. The temperature variable adsorption allowed hydrogen to overcome activation barrier of diffusion at 77 K and gave Pt/AC the highest H_2 uptake.

2. Experimental

2.1. Synthesis of adsorbents

The metal organic frameworks (MOF-5) were synthesized by a fast mixing approach [28]. The synthesis consisted of (i) adding triethylamine (99.5%, Aldrich) into an N, N′-dimethylforamide (DMF, Aldrich) solution containing zinc nitrate hexahydrate (98%, Aldrich) and 1, 4-benzenecarboxylic acid (>99%, Aldrich), and (ii) vigorously stirring at room temperature for 4 h. The resulting precipitate from the synthesis was washed repeatedly with chloroform and filtered in vacuum at room temperature. The obtained precipitate was further degassed at room temperature for 6 h and then heated at 453 K under vacuum for 12 h. The final product was white crystallites as shown in Fig. 1 with a yield of 80 (±5) % based on zinc.

The 5 wt% Pt/AC was prepared by impregnating an aqueous solution of Pt $(NH_3)_4$ $(NO_3)_2$ (Aldrich) into activated carbon (pure graphite, Norit® SX Ultra CAT) under constantly stirring at room temperature for 30 min. The prepared Pt/AC was dried in air at 423 K and then reduced in flowing H_2 at 773 K for 5 h. The final product form was fine black powder. The Pt/AC_MOF-5 was obtained by physically mixing Pt/AC and MOF-5 in a weight ratio of 1: 9 for Pt/AC to MOF-5.

2.2. Characterization of adsorbents

The crystalline structures of Pt/AC and MOF-5 were determined by X-ray diffraction (XRD) with a Philips Analytical X-Ray PW1710 diffractometer using Cu Kα radiation. The specific surface area, micropore volume, and pore width, of Pt/AC and MOF-5 were measured by an ASAP 2020 sorption meter (Micromeritics). The specific surface area was estimated by nitrogen adsorption isotherms at 77 K with the Brunauer-Emmet-Teller (BET) and Langmuir models. The micropore volume and pore width were obtained by the t-plot and Horvath–Kawazoe (H–K) method, respectively.

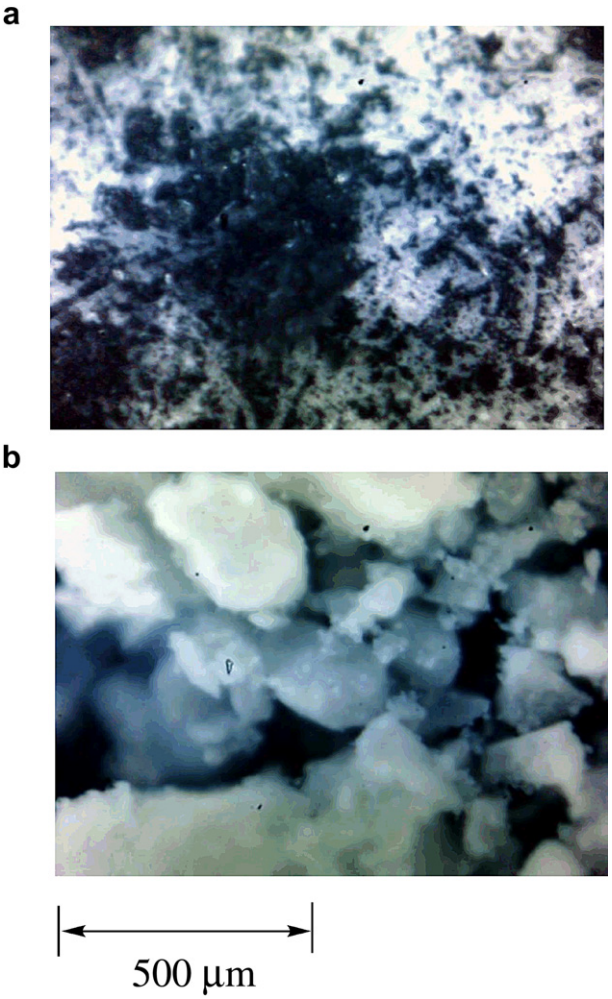

Fig. 1 – Pictures of obtained (a) activated carbon and (b) MOF-5.

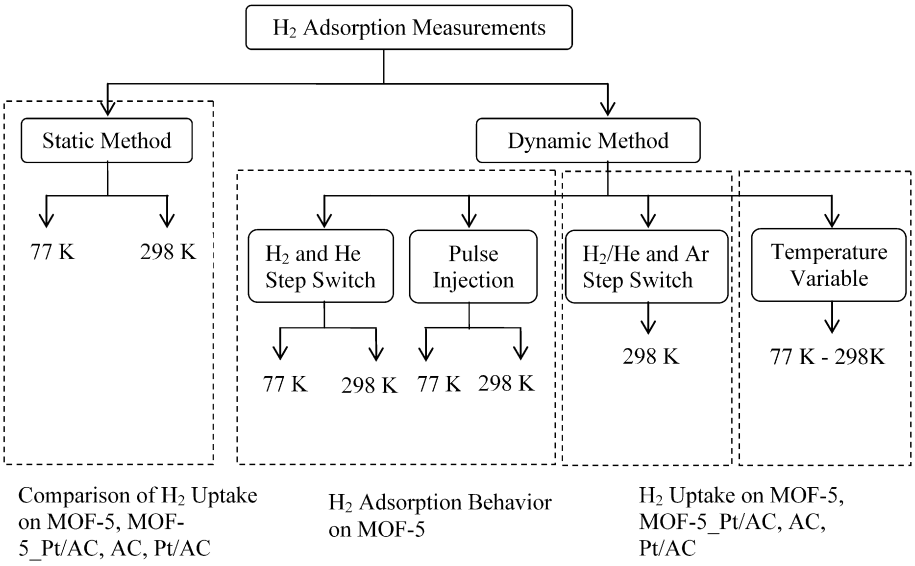

Fig. 2 – Design of adsorption experiments.

2.3. *H_2 adsorption measurements*

Fig. 2 illustrates the experimental approaches: static and dynamic adsorption methods. The static method was conducted on all adsorbents by an ASAP 2020 sorption meter at 77 and 298 K from 0 to 850 mmHg. Prior to measurements, 300(±10) mg of each adsorbent was degassed below 10 μm Hg at 523 K for 6 h and Pt-containing adsorbents were further pre-treated with H_2 at 523 K. H_2 (UHP, Praxair) was purified through a molecular sieve (Grace Davison) before use.

The dynamic method was carried out in three modes: step switch, pulse injection, and temperature variable adsorption/desorption (TVA/D). The experimental apparatus, shown in Fig. 3, consists of (i) mass flow controllers (Brooks, Model 5850E) for adjusting the flow rates of H_2, He and Ar (UHP, Praxair) streams, (ii) a quarter inch I.D. U shape tubular column filled with 100 (±5) mg of adsorbent particles which were packed with quartz wool at both ends, and (iii) a quadruple mass spectrometer (MS; Pefiffer vacuum, Omnistar GSD 301) with a differentially pumped gas inlet. The inlet of MS allowed a portion of the effluents at 1 atm to enter an ionization chamber at approximately 0.7 mbar. The mass/electron ratios, i.e. m/e, were selected for H_2 (2), HD (3), D_2 (4), He (4), and Ar (40). The calibration factor for each gaseous species, i.e. the ratio of the area under the MS profile to the amount of species injected, was determined by pulse injections of known amount of species.

Step switch was achieved by a 4-port valve which gives a step change in gaseous concentrations while maintaining the total flow rate at steady state conditions. Pulse injections were obtained by a 6-port valve which injects 5 cm^3 of H_2 into the carrier gas stream, entering to the adsorption column. The temperature variable adsorption/desorption (TVA/D) was performed by exposing the adsorbent to H_2 during cooling from 298 to 77 K and then warming from 77 to 298 K.

Isotope exchange experiments used for verification of H_2 dissociation were performed by (i) switching between H_2/D_2 (50/50) and Ar flow and (ii) a pulse injection of D_2 into H_2 gas flow through the adsorption column at 298 K. Deuterium (99.6% D_2 with 0.04% HD,) was purchased from Cambridge Isotope laboratory.

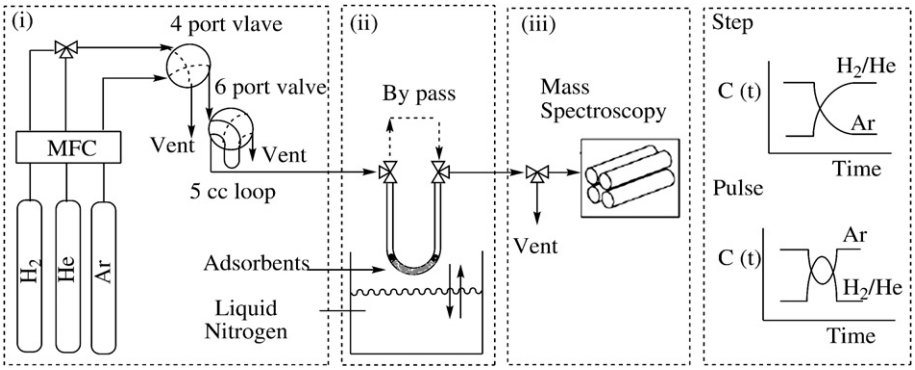

Fig. 3 – The experimental apparatus for dynamic hydrogen adsorption.

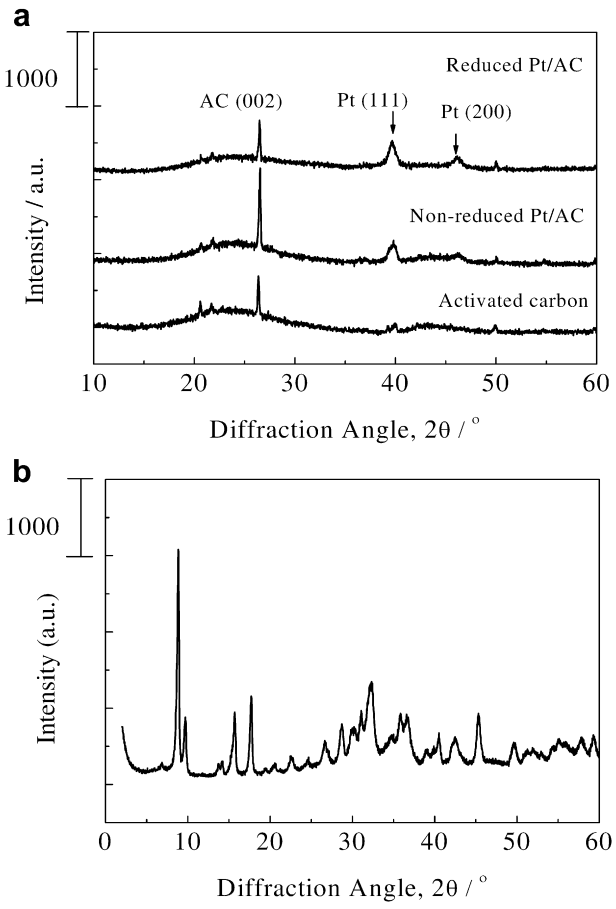

Fig. 4 – X-ray diffraction patterns of (a) activated carbon, non-reduced and reduced Pt/AC and (b) MOF-5.

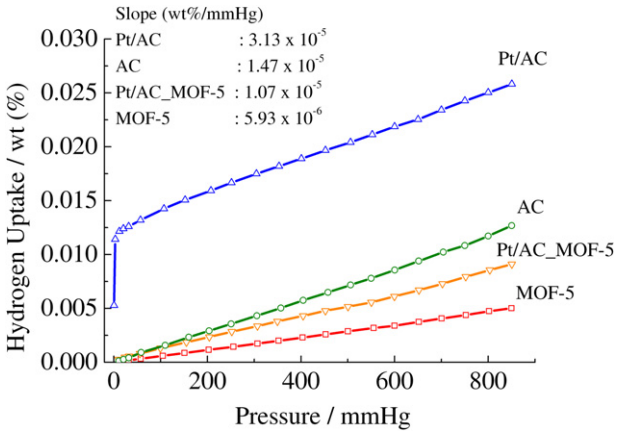

Fig. 5 – Hydrogen adsorption isotherms of carbon adsorbents and MOF-5 at 298 K.

3. Results and discussion

3.1. Characterization

Fig. 4 shows the XRD pattern for AC, Pt/AC and MOF-5.A diffraction peak at 26.4° on both AC and Pt/AC was ascribed to graphite (002) [29]. The diffraction peaks at 39.6° and 46.2° on Pt/AC were assigned to Pt (111) and Pt (200), respectively [30–32]. The XRD pattern of MOF-5 in Fig. 4(b) gave a lattice parameter of 25.8 Å, which was consistent with experimental [20,33] and simulated results [34]. The surface characterizations on these adsorbents are summarized in Table 1. The BET surface area, micropore and pore volume of MOF-5 agreed with those reported in previous literature results [20,28].

3.2. H_2 storage and adsorption isotherm

Fig. 5 shows hydrogen adsorption isotherms for all adsorbents at 298 K. All hydrogen adsorption isotherms except Pt/AC exhibited a linear behavior, obeying Henry's law [10,35]. The slope of adsorption isotherms corresponds to an adsorption equilibrium constant, which reflects the strength of interaction between adsorbate and adsorbent. The hydrogen adsorption isotherm on Pt/AC at low pressures indicated the occurrence of chemisorption, which was also observed on other Pd/AC adsorbents and AC-supported metals [36,37]. Hydrogen uptake on Pt/AC at the turning point of slope in the adsorption isotherm was 1.14×10^{-2} wt% (corresponding to a ratio 3.81 of H_{ads}/Pt), which was higher than 3.0×10^{-3} wt% (H_{ads}/Pt = 1). The high ratio of H_{ads}/Pt on Pt/AC suggested spillover of adsorbed hydrogen on Pt to the carbon surface [38]. Hydrogen uptake on all adsorbents increased in the order: MOF-5 < Pt/AC_MOF-5 < AC < Pt/AC. A relatively high Henry's constant (i.e. the slope of isotherm) for activated carbon was believed to be responsible for substantial hydrogen storage (i.e., 6.5 wt%) on carbon nanofibers [13,21]. In contrast, a low Henry's constant for MOF-5 corresponded to low hydrogen

Table 1 – Surface characterization on carbon adsorbents and MOF-5.

Sample	BET SA (m^2/g)[a]	Langmuir SA (m^2/g)[a]	Micropore volume (cm^2/g)[b]	Pore volume (cm^3/g)[c]	Medium Pore width (nm)[c]
Activated Carbon (AC)	1050	1240	0.26	0.94	3.20
5 wt% Pt/AC	990	1110	0.24	0.87	3.18
MOF-5	670	860	0.25	0.30	0.79
5 wt% Pt/AC_MOF-5	740	840	0.16	0.31	0.80

a Error = ±5%.
b From *t*-plot analysis.
c From H-K analysis.

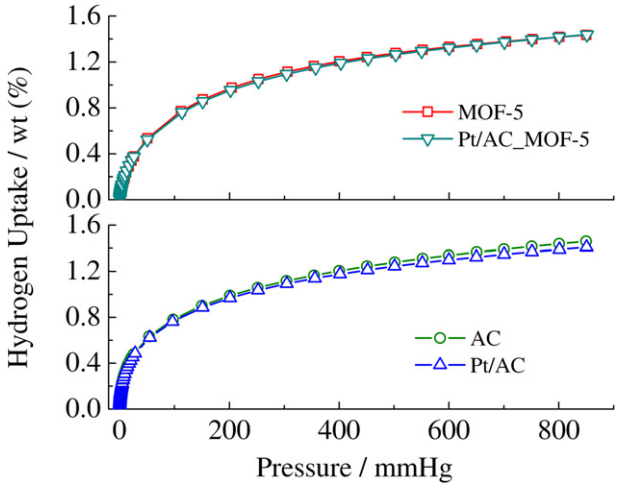

Fig. 6 – Hydrogen adsorption isotherms of carbon adsorbents and MOF-5 at 77 K.

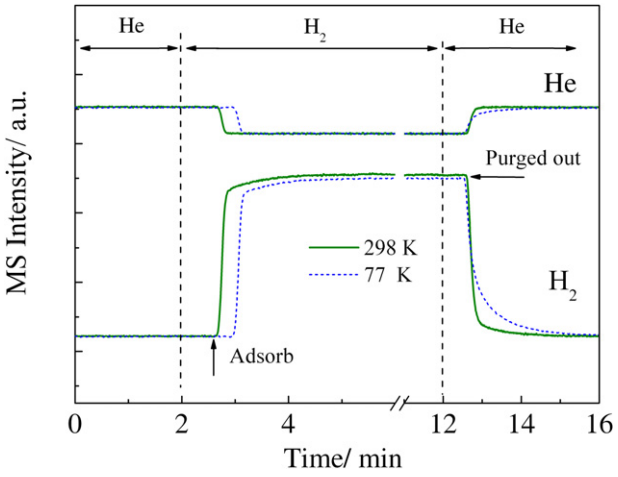

Fig. 7 – MS profiles of step switching between He and H_2 gas flow through MOF-5 at 77 and 298 K.

uptake, giving less than 0.2 wt% at pressure up to 67 bar [20] (0.3% as extrapolated in our studies). The low Henry's constant reflected that the interaction between H_2 and MOF-5 is in the form of van der Waals force. The monolayer adsorption of carbon adsorbents with a surface area 1000 m^2/g will gives a hydrogen uptake of 2.28 wt%, according to a theoretical value 2.28×10^{-3} (mass%/m^2g) [39]. Therefore, the monolayer adsorption of hydrogen on all adsorbents was not achieved.

Fig. 6 shows hydrogen adsorption isotherms on all adsorbents at 77 K. All isotherms displayed a type I (Langmuir) isotherm characteristics of microporous materials. The isotherm of MOF-5 resembled those previously reported in literature [20,25]. The saturation point of adsorption isotherms was not observed in the range of pressure investigated, implying that hydrogen uptake could be further increased by increasing H_2 pressure. The saturation point of hydrogen uptake on MOF-5 at 77 K has been reported to be 5.1 wt% [40] at the pressure above 50 bar. All hydrogen adsorption isotherms on different adsorbents, regardless of the presence or absence of Pt, at 77 K, showed the same trend with significant overlapping, suggesting a characteristic of physisorption, which exhibits low activation energy and a nonspecific interaction with adsorbents. Hydrogen uptake during physisorption can be correlated to the surface area accessible to H_2 molecules [10,20] and decreases rapidly as temperature increases.

Table 2 – The hydrogen storage capacity in the static method.

Adsorbent	Static adsorption		
	77 K	77 K (reported)	298 K (wt%)
MOF-5	1.399	1.3–1.5[20,24]	5.47E-03
Pt/AC_MOF-5	1.395		9.20E-03
AC	1.415	1.4–1.5[12,14]	1.27E-02
Pt/AC	1.369		2.58E-02

Note: error of storage capacity = ±5%.

Table 2 lists the hydrogen storage capability on all adsorbents in this study and compares with those reported in the literature. The hydrogen storage capacity normalized by the surface area at 77 K was comparable to literature values [25,41,42]. Although Pt is able to enhance hydrogen uptake on activated carbon at 298 K, such an enhancement was not observed at 77 K. This could be attributed to the absence of H_2 dissociation and subsequent spillover since dissociation of H_2 on the Pt surface has a high activation energy. It has been shown that ultrahigh vacuum treatment at 1073 K is needed to generate Pt sites for dissociative adsorption of H_2 [43].

3.3. *The dynamic method*

Fig. 7 shows the MS profiles of step switching from a stream of He to H_2 flowing into the adsorption column filled with MOF-5 at 77 and 298 K. The nearly perfect step change in the He profile indicated the absence of adsorption/desorption. In contrast, the H_2 profile rose rapidly, followed by a gradual

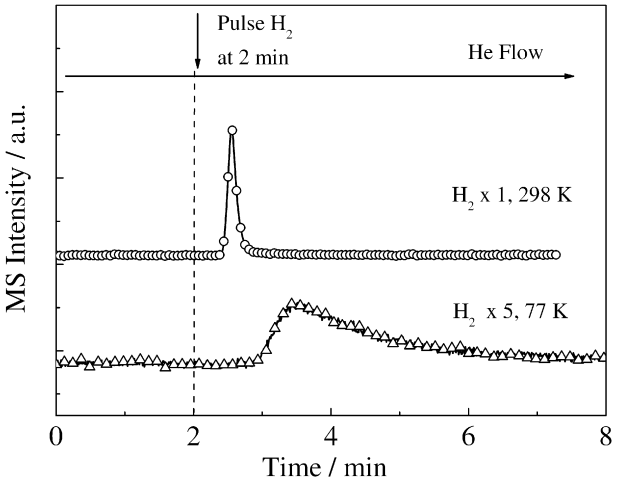

Fig. 8 – MS profiles during H_2 pulses through MOF-5 at 77 and 298 K.

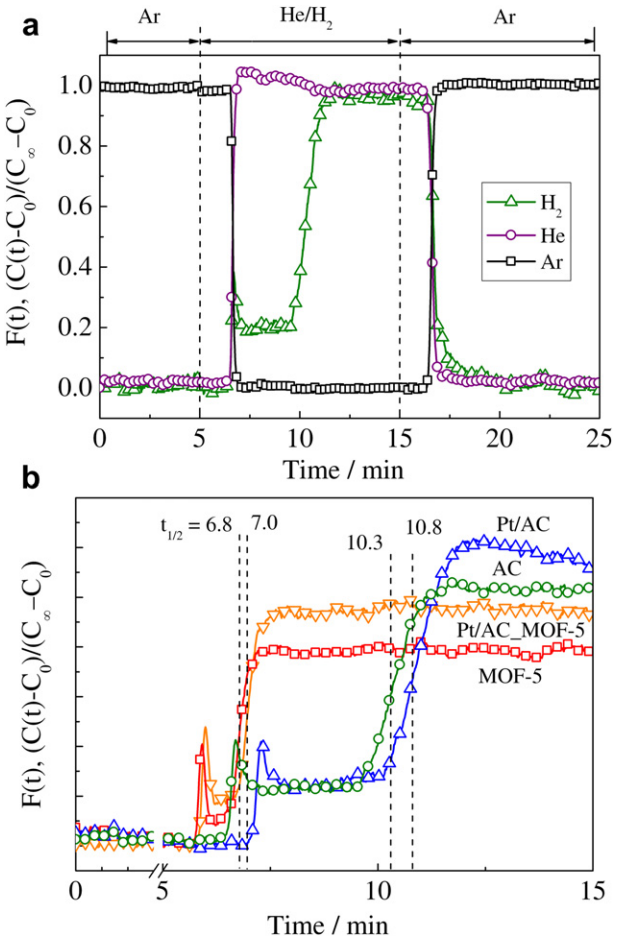

Fig. 9 – H_2, He and Ar, F(t) profiles during (a) switching between 5% H_2/He and Ar and (b) H_2 adsorption over MOF-5 (□), Pt/AC_MOF-5 (▽), AC (O), and Pt/AC (Δ) at 298 K.

increase to a final value. A similar H_2 profile with an opposite direction was also observed upon switching gas flow from H_2 to He. Decreasing temperature from 298 to 77 K prolonged trailing of the H_2 profile. The trailing profile was also observed in the pulse injection of H_2 into He at 77 K in Fig. 8. The significant trailing indicated a low rate of diffusion and a high hydrogen uptake.

To distinguish between hydrogen uptake and relative rates of hydrogen adsorption on various adsorbents, the step switch was conducted by switching a stream of H_2/He (5% H_2; He is a tracer) to Ar. Fig. 9(a) shows F(t) profiles of H_2, He, and Ar obtained during step switch at 298 K. F(t), a normalized concentration profile, is obtained by [44,45],

$$F(t) = \frac{C(t) - C_o}{C_\infty - C_o}$$

where C(t) is the concentration of H_2; C_o and C_∞ are H_2 concentration at $t = 0$ and steady state, respectively. All of adsorbents showed a sharp increase followed by a gradual increase in F(t) profiles. The first sharp increase, denoted as the first breakthrough curve, can be attributed to the hydrogen flow which passed through a loosely packed region of the adsorbent bed. The second breakthrough curve can be attributed to the hydrogen flow passing through a tightly packed region. The slope of the breakthrough curve characterizes the rate of diffusion. Higher diffusion rate would give a breakthrough curve with a sharper slope and a shorter half-time of diffusion (i.e. $t_{1/2}$). The hydrogen adsorption capacities determined by the area between the He and H_2 breakthrough curves are listed in Table 3. The hydrogen uptake increased in the order: MOF-5 < Pt/AC_MOF-5 < AC < Pt/AC. The hydrogen uptake determined from the step switch method followed the same trend as those determined by the static method at 298 K in Fig. 5 and Table 3, but the former method gave higher hydrogen storage capacity than the latter due to higher H_2 partial pressures.

Table 3 – The hydrogen uptake and release in the dynamic method.

Adsorbent	Adsorption at 298 K[a]		TVA/D[b]	
	Updake	$t_{1/2}$	Uptake at 77 K	Release at 298 K (wt%)
MOF	0.071	6.8	0.771	0.471
Pt/AC_MOF	0.103	7.0	0.796	0.489
AC	0.117	10.3	0.781	0.789
Pt/AC	0.189	10.8	1.134	1.041

a Data of Fig. 9.
b Data of Fig. 11; error: ±5%.

Fig. 10 illustrates temperature variable adsorption and desorption of H_2 (25%) in He on MOF-5. The adsorbent was exposed to H_2/He flow at 298 K. At $t = 5$ min, the adsorbent column was lowered down to 77 K in liquid nitrogen; at $t = 10$ min the adsorbent column was lifted back to 298 K. Decreasing temperature from 298 to 77 K caused a rapid drop in the H_2 profile due to increasing hydrogen adsorption; raising temperature back to 298 K caused a sharp rise due to increasing hydrogen desorption. Comparison of H_2 profiles on various adsorbents in Fig. 11 shows that Pt/AC exhibited the highest hydrogen uptake and release.

The H_2 uptake and release obtained in TVA/D are presented on Table 3. The higher uptake than release was a result of the transient nature of the experiment where hydrogen adsorbed

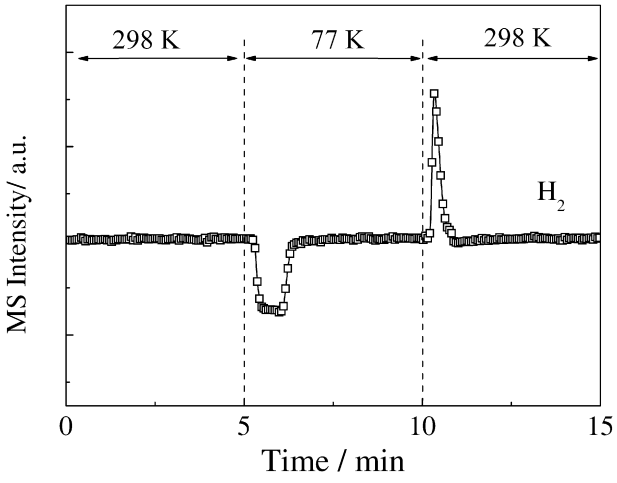

Fig. 10 – H_2 MS profiles during temperature variable adsorption and desorption on MOF-5 in 25% H_2/He.

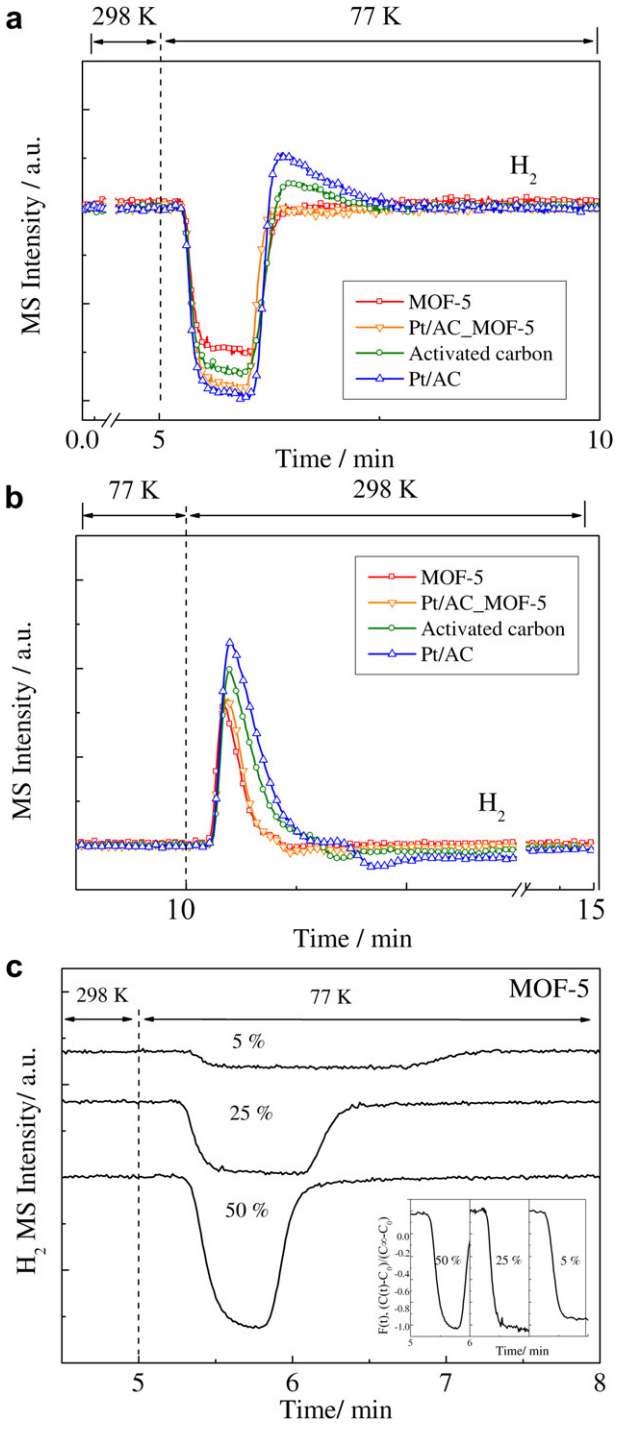

Fig. 11 – H_2 MS profiles during (a) temperature variable adsorption of H_2 at 77 K, (b) desorption at 298 K on all adsorbents in a 25% H_2/He gas stream, and (c) different conc. of H_2 adsorption on MOF-5.

during uptake was gradually released at a rate which was insufficient to give a rise in H_2 profiles. The adsorption kinetics was characterized by the slope of MS adsorption profile with different concentrations of H_2, e.g. MOF-5 in Fig. 11(c). Higher H_2 concentrations gave a steeper MS profile (inset of Fig. 11(c)), indicating higher rates of adsorption and diffusion. Comparison of hydrogen uptake obtained by dynamic methods in

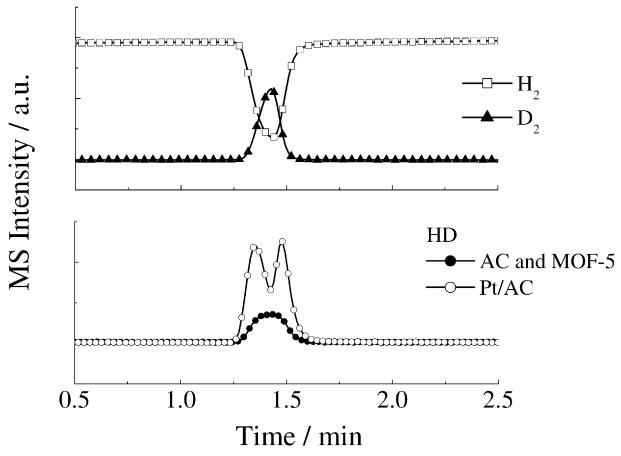

Fig. 12 – Isotope exchange of deuterium during pulse injection of D_2 in H_2 flow through Pt/AC, AC and MOF-5 at 298 K.

Table 3 shows that the TVA/D approach resulted in higher hydrogen storage on Pt/AC, suggesting that thermal energy possessed by H_2 at 298 K may allow it to overcome the activation barrier for H_2 adsorption during cooling of the adsorbent bed to 77 K.

The higher H_2 uptake of Pt/AC can be attributed to the dissociative adsorption of hydrogen followed by spillover of adsorbed hydrogen from Pt to AC sites. The dissociative adsorption of hydrogen on Pt/AC can be further evidenced by the formation of two humps of HD during the pulse injection of D_2 into H_2 in Fig. 12. The two-hump HD transient response has been observed on pulsing D_2 to H_2 over Rh/SiO_2 catalysts [46]. The observed equal size of two humps in HD response is due to the rapid dissociation of H_2 and D_2 followed by the combination of adsorbed H and D. The rapid dissociative hydrogen and deuterium adsorption allowed the coverage of adsorbed H and D on adsorbents closely follow the concentration of H_2 and D_2. The peak of the hump would occur at nearly equal coverage of H and D (θ_H and θ_D), assuming that $r_{HD} = k \cdot \theta_H \cdot \theta_D$. As the coverage of H and D deviates from equal coverage, r_{HD} decreases.

Hydrogen dissociation on Pt sites and subsequent spillover from Pt to carbon matrix has been reported [47]. Crystallite face of Pt (111) has the lowest surface energy [48,49] and adsorbs hydrogen with heat of adsorption energy about 237 ($kJmol^{-1}$) [38]. These hydrogen have been shown to be responsible for H_2 spillover and oxidation reactions [50]. At a constant temperature, hydrogen spillover can be a reversible process which allows adsorbed hydrogen to reversely migrate from carbon surface back to Pt surface for desorption [51]. The reversible nature suggested that the spillover process has lower activation energy than H_2 chemisorption. The activation energy of H_2 spillover has been determined to be less than 10 $kJmol^{-1}$ [52]. The reversed spillover process may contribute to overshoot of H_2 MS profiles during hydrogen desorption on Pt/AC in Fig. 11(a). The spillover and reversed spillover process did not occur on the physical mixture of Pt/AC and MOF, as evidenced by its low hydrogen storage capacity. This result suggested that adsorbed hydrogen on the carbon surface was not able to transfer via

a physical contact between carbon and MOF surfaces, confirming the results of a number of previous studies [37].

4. Conclusions

The hydrogen adsorption isotherm on all adsorbents showed type I (Langmuir) isotherm characteristics of microporous materials at 77 K, giving a hydrogen storage capacity in the range of 1.3–1.4 wt%. The results suggested that hydrogen adsorption on these materials was in the form of physisorption. At 298 K, hydrogen adsorption capacities on all adsorbents gave a linear function of pressure with the capacity increasing in the order: MOF-5 < Pt/AC_MOF-5 < AC < Pt/AC. The dynamic method at 298 K showed that small Pt/AC particles gave a close packed bed, slowing down the diffusion of H_2 to the adsorption sites and exhibiting a breakthrough curve with a smaller slope than those resulted from the loosely bed packed by large MOF particles. Pt/AC exhibited a significantly higher hydrogen storage capacity during temperature variable adsorption than dynamic step and static adsorption at 298 K, suggesting that hydrogen adsorption during TVA/D involves two steps: (i) the H_2 dissociative step at high temperature and (ii) the subsequent spillover step. Temperature variable adsorption can serve as an approach to enhance the adsorption process which involves a number of steps with different activation energies.

Acknowledgements

The authors are grateful to the financial support from U.S. Department of Defense through a subcontract from Ovonic Hydrogen System, LLC, R7712-Univ of Akron.

REFERENCES

[1] Lowell S, Shields JE. Powder surface area and porosity. Chapman & Hall; 1991.
[2] Xu Xiaochun, Zheng Jian, Song C. Dynamic measurement of hydrogen storage/release properties of Mg doped with Pd nanoparticles using a tapered-element oscillating microbalance under flow conditions. Energy Fuels 2005;19:2107.
[3] Jiang Jinhua, Gao Qiuming, Zheng Zhoujun, Xia Kaisheng, Hu J. Enhanced room temperature hydrogen storage capacity of hollow nitrogen-containing carbon spheres. Int J Hydrogen Energy 2010;35:210–6.
[4] Geng Hong-Zhang, Kim Tae Hyung, Lim Seong Chu, Jeong Hae-Kyung, Jin Mei Hua, Jo Young Woo, et al. Hydrogen storage in microwave-treated multi-walled carbon nanotubes. Int J Hydrogen Energy 2010;35:2073–82.
[5] Wua Huimin, Wexler David, Ranjbartoreh Ali Reza, Liu Huakun, Wang G. Chemical processing of double-walled carbon nanotubes for enhanced hydrogen storage. Int J Hydrogen Energy 2010;35:1–5.
[6] Rowsell Jesse LC, Yaghi OM. Strategies for hydrogen storage in metal–organic frameworks. Angew Chem Int Ed 2005;44:4670–9.
[7] Hirscher Michael, Panella B. Hydrogen storage in metal–organic frameworks. Scripta Materialia 2007;56:809–12.
[8] Li Jinping, Cheng Shaojuan, Zhao Qiang, Long Peipei, Dong J. Synthesis and hydrogen-storage behavior of metal–organic framework MOF-5. Int J Hydrogen Energy 2009;34:1377–82.
[9] Dinca Mircea, Yu Anta F, Long JR. Microporous metal-organic frameworks Incorporating 1,4-Benzeneditetrazolate: Syntheses, structures, and hydrogen storage properties. J Am Chem Soc 2006;128(27):8904–13.
[10] Kojima Yoshitsugu, Kawai Yasuaki, Koiwai Akihiko, Suzuki Nobuaki, Haga Tetstuya, Hioki Tatsumi, et al. Hydrogen adsorption and desorption by carbon materials. J Alloys Compd 2006;421:204–8.
[11] Ströbel R, Jörissen L, Schliermann T, Trapp V, Schütz W, Bohmhammel K, et al. Hydrogen adsorption on carbon materials. J Power Sources 1999;84:221–4.
[12] Zhou Li, Zhou Yaping, Sun Y. Studies on the mechanism and capacity of hydrogen uptake by physisorption-based materials. Int J Hydrogen Energy 2006;31:259–64.
[13] Browning Darren J, Gerrard Mark L, Lakeman J Barry, Mellor Ian M, Mortimer Roger J, Turpin MC. Studies into the storage of hydrogen in carbon nanofibers: proposal of a possible reaction mechanism. Nano Lett 2002;2(3):201–5.
[14] Kadono K, Kajiura H, Shiraishi M. Dense hydrogen adsorption on carbon subnanopores at 77 K. Appl Phys Lett 2003;83(16):3392–4.
[15] Poirier E, Chahine R, Bose TK. Hydrogen adsorption in carbon nanostructures. Int J Hydrogen Energy 2001;26:831–5.
[16] Wong-Foy Antek G, Matzger Adam J, Yaghi OM. Exceptional H_2 saturation uptake in microporous metal-organic frameworks. J Am Chem Soc 2006;128:3494–5.
[17] de la Casa-Lillo MA, Lamari-Darkrim F, Cazorla-Amorós D, Linares-Solano A. Hydrogen storage in activated carbons and activated carbon fibers. J Phys Chem B 2002;106:10930–4.
[18] Ritschel M, Uhlemann M, Gutfleisch O, Leonhardt A, Graff A, Täschner Ch, et al. Hydrogen storage in different carbon nanostructures. Appl Phys Lett 2002;80:2985.
[19] Xu W-C, Takahashi K, Matsuo Y, Hattori Y, Kumagai M, Ishiyama S, et al. Investigation of hydrogen storage capacity of various carbon materials. Int J Hydrogen Energy 2007;32:2504–12.
[20] Panella B, Hirscher M. Hydrogen physisorption in metal-organic porous crystals. Adv Mater (Weinheim Ger) 2005;17(5):538–41.
[21] Lueking AD, Yang RT. Hydrogen spillover to enhance hydrogen storage – study of the effect of carbon physicochemical properties. Appl Catal A Gen 2004;265(2):259–68.
[22] Yoo E, Gao L, Komatsu T, Yagai N, Arai K, Yamazaki T, et al. Atomic hydrogen storage in carbon nanotubes promoted by metal catalysts. J Phys Chem B 2004;108(49):18903–7.
[23] Zacharia R, Kim KY, Fazle Kibria AKM, Nahm KS. Enhancement of hydrogen storage capacity of carbon nanotubes via spill-over from vanadium and palladium nanoparticles. Chem Phys Lett 2005;412(4–6):369–75.
[24] Liu Y-Y, Zeng J-L, Zhang J, Xu F, Sun L- X. Improved hydrogen storage in the modified metal-organic frameworks by hydrogen spillover effect. Int J Hydrogen Energy 2007;32(16):4005–10.
[25] Li Yingwei, Yang RT. Significantly enhanced hydrogen storage in metal-organic frameworks via spillover. J Am Chem Soc 2006;128(3):726–7.
[26] Li Yingwei, Yang RT. Gas adsorption and storage in metal-organic framework MOF-177. Langmuir 2007;23:12937–44.
[27] Miller Michael A, Wang Cheng-Yu, Merrill GN. Experimental and theoretical investigation into hydrogen storage via spillover in IRMOF-8. J Phys Chem C 2009;113:3222–31.
[28] Huang L, Wang H, Chen J, Wang Z, Sun J, Zhao D, et al. Synthesis, morphology control, and properties of porous metal-organic coordination polymers. Microporous Mesoporous Mater 2003;58(2):105–14.
[29] Sun G, Li X, Qu Y, Wang X, Yan H, Zhang Y. Preparation and characterization of graphite nanosheets from detonation technique. Mater Lett 2008;62(4–5):703–6.

[30] Wakayama H, Fukushima Y. Porous platinum fibers synthesized using supercritical fluid. Chem Commun 1999; (4):391–2.
[31] Huang S-Y, Chang S-M, Yeh C-t. Characterization of surface composition of platinum and ruthenium nanoalloys dispersed on active carbon. J Phys Chem B 2006;110(1): 234–9.
[32] Chen S, Xu R, Huang H, Yi F, Zhou X, Zeng H. Reduction-adsorption behavior of platinum ions on activated carbon fibers. J Mater Sci 2007;42(23):9572–81.
[33] Li Hailian, Eddaoudi Mohamed, O'Keeffe M, Yaghi OM. Design and synthesis of an exceptionally stable and highly porous metal-organic framework. Nature 1999;402:276–9.
[34] Eddaoudi M, Moler D, Li H, Reineke TM, M., O'Keeffe, et al. Acc Chem Res 2001;34:319.
[35] Panella B, Hirscher M, Roth S. Hydrogen adsorption in different carbon nanostructures. Carbon 2005;43(10): 2209–14.
[36] Puddephatt RJ. Platinum(IV) hydride chemistry. Coord Chem Rev 2001;219–221(1):157–85.
[37] Anthony J, Lachawiec J, Qi Gongshin, Yang RT. Hydrogen storage in nanostructured carbons by spillover: bridge-building enhancement. Langmuir 2005;21:11418–24.
[38] Zolt'an Pa'al, Menon PG, editors. Hydrogen effects in catalysis, fundamentals and practical applications. Marcel Dekker; 1988.
[39] Zuttel A, Sudan P, Mauron P, Wenger P. Model for the hydrogen adsorption on carbon nanostructures. Appl Phys A 2004;78(7):941–6.
[40] Panella Barbara, Hirscher Michael, Pütter Hermann, Müller U. Hydrogen adsorption in metal–organic frameworks: Cu-MOFs and Zn-MOFs compared. Adv Funct Mater 2006;16:520–4.
[41] Schlapbach Louis, Züttel A. Hydrogen-storage materials for mobile applications. Nature 2001;414:353–8.
[42] Nijkamp MG, Raaymakers JEMJ, van Dillen AJ, Jong KPD. Hydrogen storage using physisorption–materials demands. Appl Phys A 2001;72:619–23.
[43] Nishiyama Satoru, Yoshida Tsuyoshi, Kimura Kazuki, Tsuruya Shigeru, Masai M. Generation of active sites over Pt powder catalysts by UHV treatment Temperature programmed desorption study. Catal Today 1996;28:205–14.
[44] Balakos MW, Chuang Steven SC, Srinivas G, Brundage MA. Infrared study of the dynamics of adsorbed species during CO hydrogenation. J Catal 1995;157(1):51–65.
[45] Krishnamurthy R, Chuang SSC, W. BM. Step and pulse transient studies of Ir-observable adsorbates during NO and CO reaction on Rh/SiO_2. J Catal 1995;157(2):512–22.
[46] Hedrick Scott A, Chuang Steven SC, Brundage MA. Deuterium pulse transient analysis for determination of heterogeneous ethylene hydroformylation mechanistic parameters. J Catal 1999;185:73–90.
[47] Robell Andrew J, Ballou EV, Boudart M. Surface diffusion of hydrogen on carbon. J Phys Chem B 1964;68:2748–53.
[48] Kinoshita K, Swnehart P. Role of platinum surface morphology on hydrogen adsorption isother – IV. Electrochimica Acta 1975;20:101–7.
[49] Arboleda Jr Nelson B, Kasai Hideaki, Diño Wilson A, Nakanishi H. Quantum dynamics study on the interaction of H_2 on a Pt(111) surface. Thin Solid Films 2006;509:227–9.
[50] Gorodetskii VV, Sametova AA, Matveev AV, Tapilin VM. From single crystals to supported nanoparticles in experimental and theoretical studies of H_2 oxidation over platinum metals (Pt, Pd): Intermediates, surface waves and spillover. Catal Today 2009;144:219–34.
[51] Li Yingwei, Yang RT. Hydrogen storage on platinum nanoparticles doped on superactivated carbon. J Phys Chem C 2007;111:11086–94.
[52] Yang Ralph T, Wang Y. Catalyzed hydrogen spillover for hydrogen storage. J Am Chem Soc 2009;131:4224–6.